Nonlinear dynamics of damped and driven velocity-dependent systems

A. Venkatesan and M. Lakshmanan
Centre for Nonlinear Dynamics, Department of Physics, Bharathidasan University, Tiruchirappalli 620 024, India
(Received 6 December 1996)

In this paper, the nonlinear dynamics of certain damped and forced versions of velocity-dependent potential systems, namely, (i) the motion of a particle on a rotating parabola and (ii) a nonlinear harmonic oscillator, is considered. Various bifurcations such as symmetry breaking, period doubling, intermittency, crises, and antimonotonicity are reported. We also investigate the transition from two-frequency quasiperiodicity to chaotic behavior in a model for the quasiperiodically driven rotating parabola system. As the driving parameter is increased, the route to chaos takes place in four distinct stages. The first stage is a torus doubling bifurcation. The second stage is a merging of doubled torus. The third stage is a transition from the merged torus to a strange nonchaotic attractor. The final stage is a transition from the strange nonchaotic attractor to a geometrically similar chaotic attractor. [S1063-651X(97)00505-9]

PACS number(s): 05.45.+b

I. INTRODUCTION

In this paper, we consider the dynamics of a class of nonpolynomial oscillators governed by the equations of motion

$$(1+\lambda x^2)\ddot{x}+\lambda x\dot{x}^2+\omega_0^2 x=0 \tag{1}$$

and

$$(1-\lambda x^2)\ddot{x}+\lambda x\dot{x}^2+\omega_0^2 x=0, \quad \left(\cdot=\frac{d}{dt}\right) \tag{2}$$

and subjected to additional linear damping and periodic forcing.

In particular, Eq. (1) is a well-known model [1–3] for the analysis of inherently nonlinear phenomena in a nongeneric mechanical system corresponding to the Lagrangian

$$L=\tfrac{1}{2}[(1+\lambda x^2)\dot{x}^2-\omega_0^2 x^2], \tag{3}$$

whence the Hamiltonian is

$$H=\tfrac{1}{2}[p^2(1+\lambda x^2)^{-1}+\omega_0^2 x^2],$$

and the canonical momentum is

$$p=\dot{x}(1+\lambda x^2).$$

A mechanical setup for this case is that of the motion of a particle of mass m sliding freely on a wire described by the parabola $z=\sqrt{\lambda/2}x^2$, which rotates with a constant angular velocity $[\Omega=\Omega_0=(-\omega_0^2+g\sqrt{\lambda})^{1/2}]$ about its z axis as shown in Fig. 1. A physical realization of this model is that of a man riding a motor bike on a rotating parabolic well in a circus. When $\omega_0^2>0$, physically realizable solutions to Eq. (1) can be expressed in terms of elliptic integrals.

Equation (2) corresponds to a velocity-dependent potential-type nonlinear oscillator, exhibiting amplitude-dependent simple harmonic oscillations [3–5]. It is a model system corresponding to the oscillator version describing pion-pion interaction with the Lagrangian [6]

$$L=\frac{1}{2}\left[\frac{\dot{x}^2+\omega_0^2 x^2}{1-\lambda x^2}\right], \tag{4}$$

and the corresponding Hamiltonian is

$$H=\tfrac{1}{2}[p^2(1-\lambda x^2)+\omega_0^2 x^2(1-\lambda x^2)^{-1}],$$

with

$$p=\dot{x}(1-\lambda x^2)^{-1}.$$

Also, a perturbative analysis of this model can reproduce the exact solution for all values of the coupling parameter λ [5]. The corresponding field system for Eq. (4) has an interestingly simple harmonic traveling wave solution. In the massless case, this is an isoscalar analogue of the chiral invariant $SU(2)\otimes SU(2)$ Lagrangian in the Gasiorowicz-Geffen coordinates [7].

It is of considerable physical interest to consider the nonlinear dynamics of Eqs. (1) and (2) under the influence of

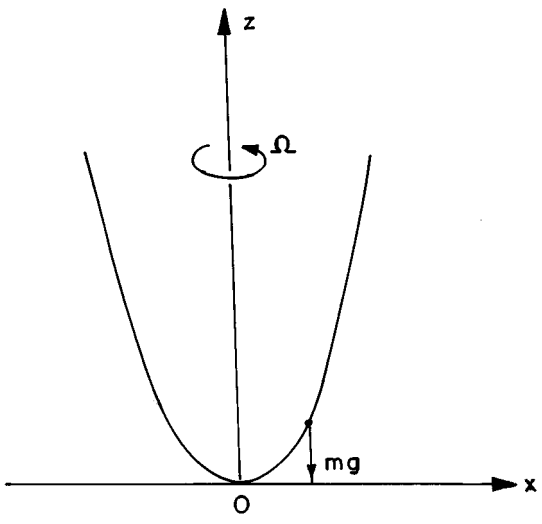

FIG. 1. Particle on a rotating parabola defined by $z=\sqrt{\lambda/2}x^2$.

additional damping and external periodic forces so that the equations of the motion become

$$(1+\lambda x^2)\ddot{x}+\lambda x\dot{x}^2+\omega_0^2 x+\alpha\dot{x}=f\ \cos\omega t \tag{5}$$

and

$$\ddot{x}+\frac{(\lambda x\dot{x}^2+\omega_0^2 x)}{(1-\lambda x^2)}+\alpha\dot{x}=f\ \cos\omega t, \tag{6}$$

respectively, in place of Eqs. (1) and (2). In addition, we consider the system shown in Fig. 1, when the angular velocity is parametrically varying as [2]

$$\Omega=\Omega_0(1+\epsilon\ \cos\omega_p t). \tag{7}$$

Then the equation of motion can be rewritten as

$$(1+\lambda x^2)\ddot{x}+\lambda x\dot{x}^2+\omega_0^2 x-\Omega_0^2[2\epsilon\ \cos\omega_p t + 0.5\epsilon^2(1+\cos 2\omega_p t)]x+\alpha\dot{x}=f\ \cos\omega_e t, \tag{8}$$

where ω_e is the frequency of the external force.

In particular, we wish to make a detailed investigation of the dynamics of the mechanical system (5) and investigate the existence of a rich variety of bifurcations as the external forcing parameter is varied while all other parameters are fixed. Specifically, we would like to present a detailed account of the various bifurcations such as symmetry breaking, period doubling, periodic windows, intermittency, and antimonotonicity, exhibited by the system (5) as the parameter changes. We also investigate the transition from two-frequency quasiperiodicity to chaotic behavior in the system (8). As the parameter is increased, the route to chaos takes place in four distinct phases. The first phase is a torus-doubling bifurcation. The second phase corresponds to the doubled torus merging into a single torus. The third phase is a transition from the merged torus to a strange nonchaotic attractor. The final phase is a transition from the strange nonchaotic attractor to a geometrically similar chaotic attractor. Finally, we wish to present briefly the bifurcation routes and chaotic dynamics of system (6). In particular, the existence of symmetry breaking, period doubling, antimonotonicity, and crises bifurcations are reported.

II. CHAOTIC DYNAMICS OF THE MOTION OF A PARTICLE ON A ROTATING PARABOLA UNDER THE INFLUENCE OF DAMPED AND DRIVEN FORCES

To be concrete, we consider the dynamics of Eq. (5) where we fix the values of the parameters as $\omega_0^2=0.25$, $\lambda=0.5$, $\alpha=0.1$, $\Omega^2=\Omega_0^2=6.7$, and $\omega=1.0$ and vary the value of the forcing parameter f. At low values of the forcing parameter, the response asymptotically approaches a stable fixed point. As the forcing parameter is further increased, a stable symmetrical limit cycle occurs at $f=0.012$. As we slowly increase the value of f, the symmetric solution bifurcates into a limit cycle that exhibits asymmetrical behavior at

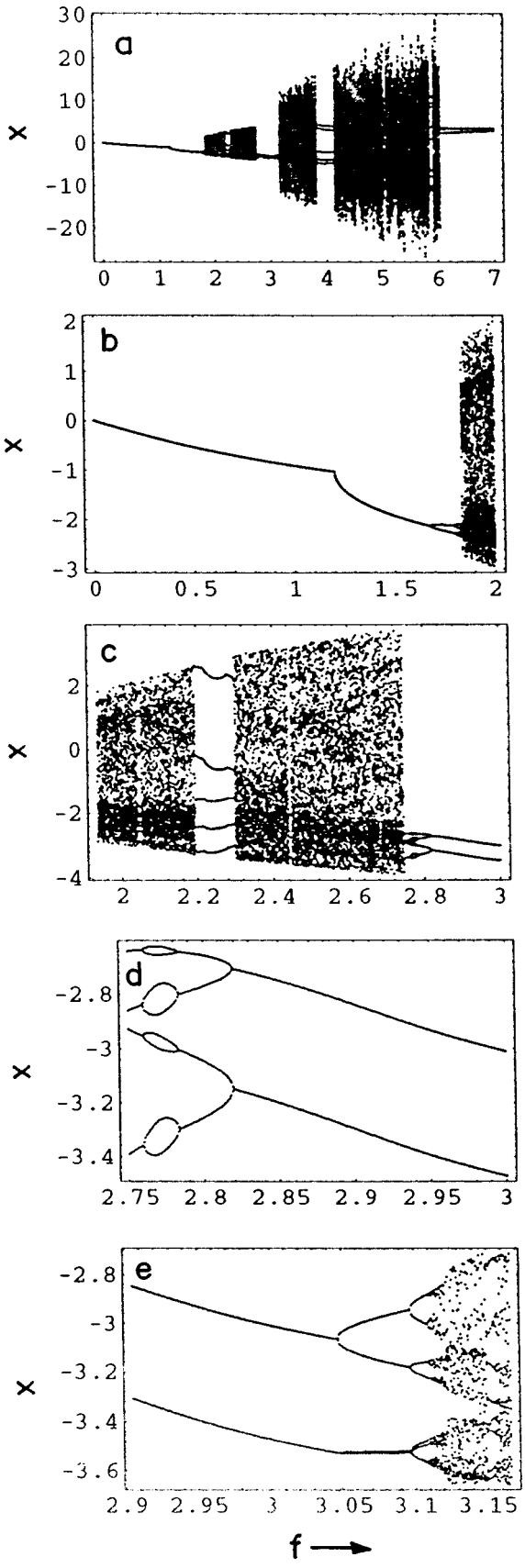

FIG. 2. Bifurcation diagram of the system (5) for $x(t)$ vs f, (a) $f\in(0.0,7.0)$; (b) symmetry-breaking and period-doubling bifurcations for $f\in(0.0,2.0)$; (c) periodic windows in the interval $f\in(2.0,3.0)$; (d),(e) a reverse period-2 bubble for $f\in(2.75,3.15)$. The other parameters are $\omega_0^2=0.25$, $\lambda=0.5$, $\alpha=0.2$, and $\omega=1.0$.

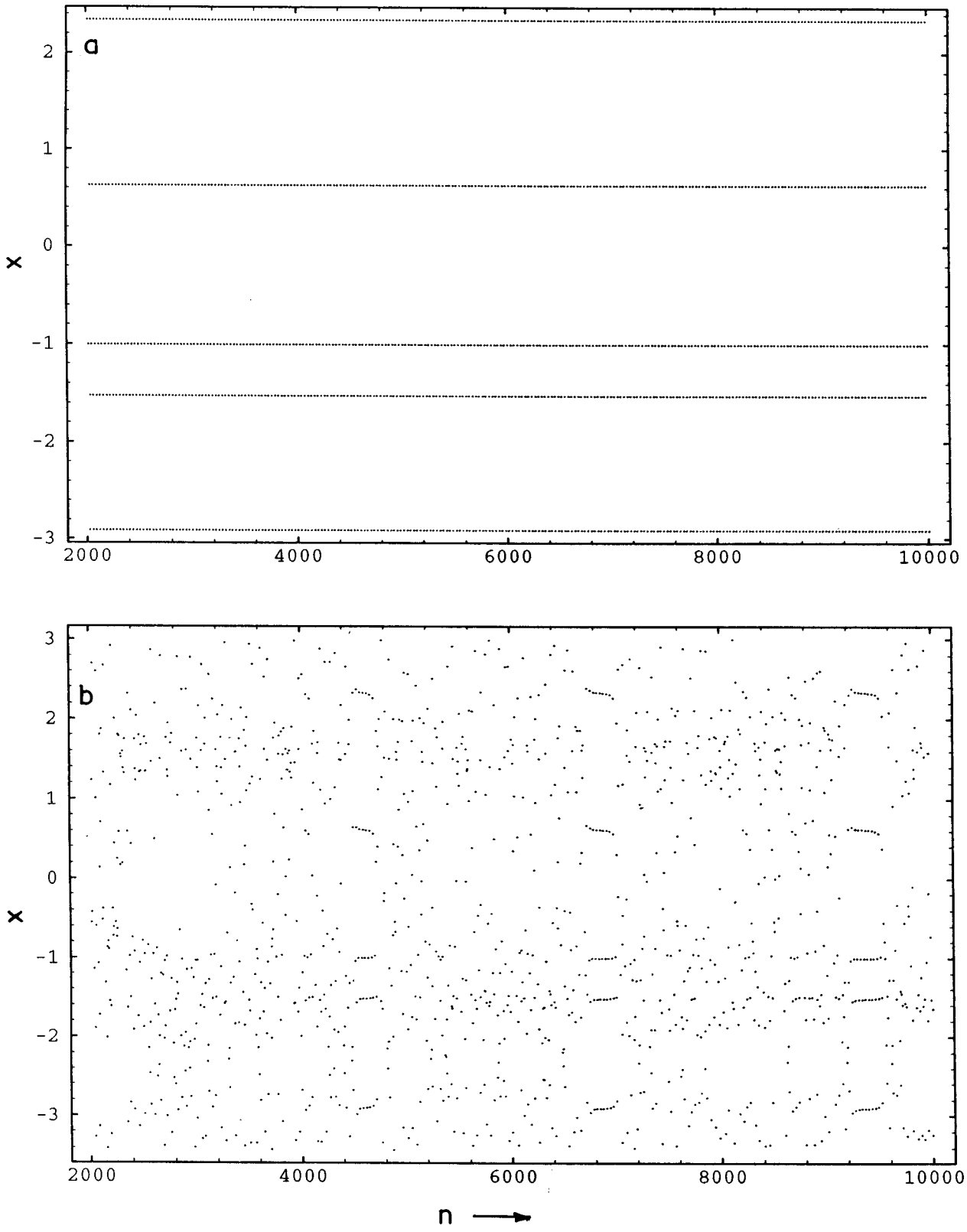

FIG. 3. Time series x_n containing laminar parts vs the number of cycles n. (a) Period-5 orbit at $f=2.2993$; (b) intermittent chaos at $f=2.2995$.

$f=1.213$. Even though the velocity-dependent potential energy of this system is symmetric, the actual behavior of the response is not symmetric, leading to dynamical symmetry breaking similar to the one that occurs in a Duffing oscillator [8,9].

A. Feigenbaum scenario

As the parameter f is further increased, a period-doubled orbit appears and the original limit cycle becomes unstable at $f=1.689$. As we increase the value of f further, this period-2

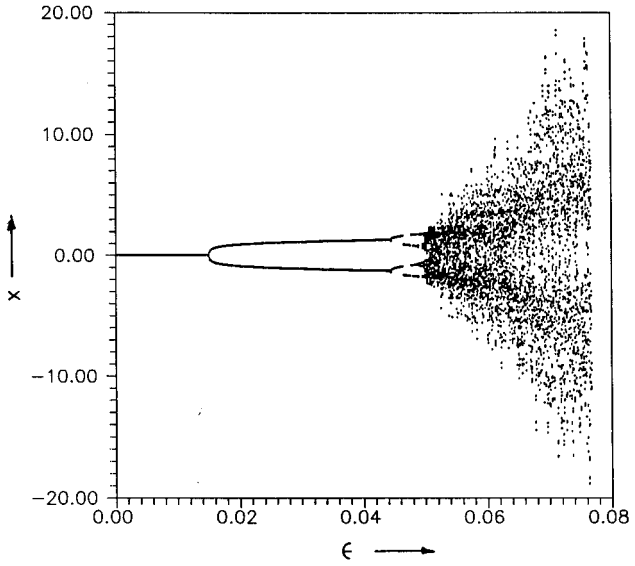

FIG. 4. Bifurcation diagram of Eq. (8) for $x(t)$ vs ϵ: $\epsilon \in (0,0.08)$. The other parameters are $\omega_0^2=0.25$, $\lambda=0.5$, $\alpha=0.2$, $\omega_p=1$, $\Omega_0^2=6.7$, and $f=\omega_e=0$.

orbit flips to a period-4 orbit at $f=1.823$, which then bifurcates to a period-8 orbit at $f=1.874$ and so on, as shown in the bifurcation diagram, Fig. 2. This infinite sequence ends up in chaotic motion in the standard way. Of course, one can verify that the bifurcation sequence is associated with the Feigenbaum universal constant [10]. Further increase in the value of f leads to periodic windows and further complex behaviors (as depicted in Fig. 2), which are discussed below.

B. Periodic windows and intermittency

In addition to the obvious chaotic orbits, Fig. 2 also shows that there are certain ranges of the parameters where periodic behavior appears that is essentially due to tangent bifurcation. For example, the widest range is occupied by the period-5 orbit in the interval $2.199<f<2.301$ and reverse period-2 bubble in the interval $2.731<f<3.153$.

In the intermittency transition [11], when the value of the control parameter is greater than a critical value, the periodic orbit is replaced by a chaotic orbit. An example of this phenomenon is illustrated in the interval $2.29<f<2.301$. From Fig. 3, we see that just before the value $f_{*5}=2.2994$, we have a stable period-5 orbit, while just after f_{*5}, there is chaos. Thus as the parameter f is increased through f_{*5}, we have an intermittency transition from a periodic to a chaotic attractor. For f slightly greater than f_{*5}, there are finite stretches of time during which the orbit closely resembles the orbit for $f<f_{*5}$, but this regular (approximately periodic) behavior is intermittently interrupted by finite duration ''bursts'' in which the orbit behaves in a decidedly different manner.

C. Antimonotonicity

Recently Yorke and co-workers [12,13] have shown that antimonotonicity, inevitable reversals of period-doubling cascades [14,15], is a fundamental phenomenon for a large class of nonlinear systems. One finds that periodic orbits are not only created but also destroyed when one increases the control parameter monotonically (smoothly) in any neighborhood of a homoclinic tangency value. Now we wish to point out that for the present problem, antimonotonicity can be observed in one way by looking at the bifurcation diagram, Fig. 2, in the range $2.731<f<3.153$. As f is increased, the chaotic behavior is followed by an ''unusual'' period-4 orbit. The period-8 orbit appears and disappears due to pitchfork bifurcation in the range $2.753<f<2.775$, followed by a reverse period-doubling bifurcation whence a period-4 orbit and then a period-2 orbit appear. Further, it is followed by a complete period-doubling sequence leading to chaotic oscillations. Such a pattern is called a reverse period-2 bubble. We also notice that in the above range the reverse period cascades of the period-2 orbit starts in an unusual way [16], however, this is followed by the standard period-doubling sequence.

III. CHAOTIC DYNAMICS OF THE MOTION OF A PARTICLE ON A ROTATING PARABOLA UNDER THE INFLUENCE OF DAMPED, DRIVEN AND PARAMETRIC FORCING

So far, we have discussed the dynamics of the system (5) with constant angular velocity $\Omega=\Omega_0$ $[=(-\omega_0^2+g\sqrt{\lambda})^{1/2})]$. Now we consider the system (8), which has a parametrically varying angular velocity instead of the constant angular velocity Ω as given in Eq. (7). Equation (8) can be equivalently rewritten as

$$\dot{x}=y,$$

$$\dot{y}=\left[\frac{(-\lambda xy^2-\{\omega_0^2-\Omega_0^2[2\epsilon\cos\phi+0.5\epsilon^2(1+\cos 2\phi)]\}x-\alpha y+f\cos\theta)}{(1+\lambda x^2)}\right], \tag{9}$$

$$\dot{\phi}=\omega_p,$$

$$\dot{\theta}=\omega_e,$$

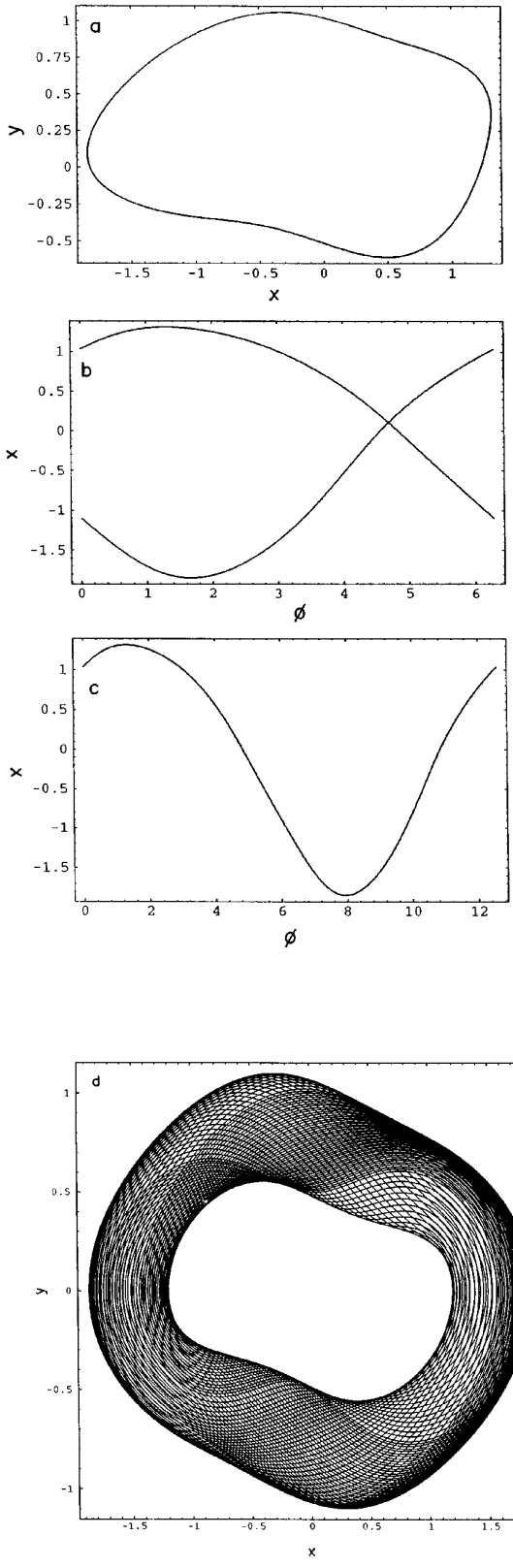

FIG. 5. Projection of the two-frequency quasiperiodic attractors of Eq. (8) for $\epsilon = 0.03$: (a) Poincaré map in the $(x\text{-}y)$ plane; (b) Poincaré map with ϕ mod 2π in the (x, ϕ) plane; (c) same as (b) except ϕ mod 4π during computation; (d) trajectory in the $(x\text{-}y)$ plane. The other parameters are $\omega_0^2 = 0.25$, $\lambda = 0.5$, $\alpha = 0.2$, $\omega_p = 1.0$, $\Omega_0^2 = 6.7$, $f = 0.32$, and $\omega_e = 0.991$.

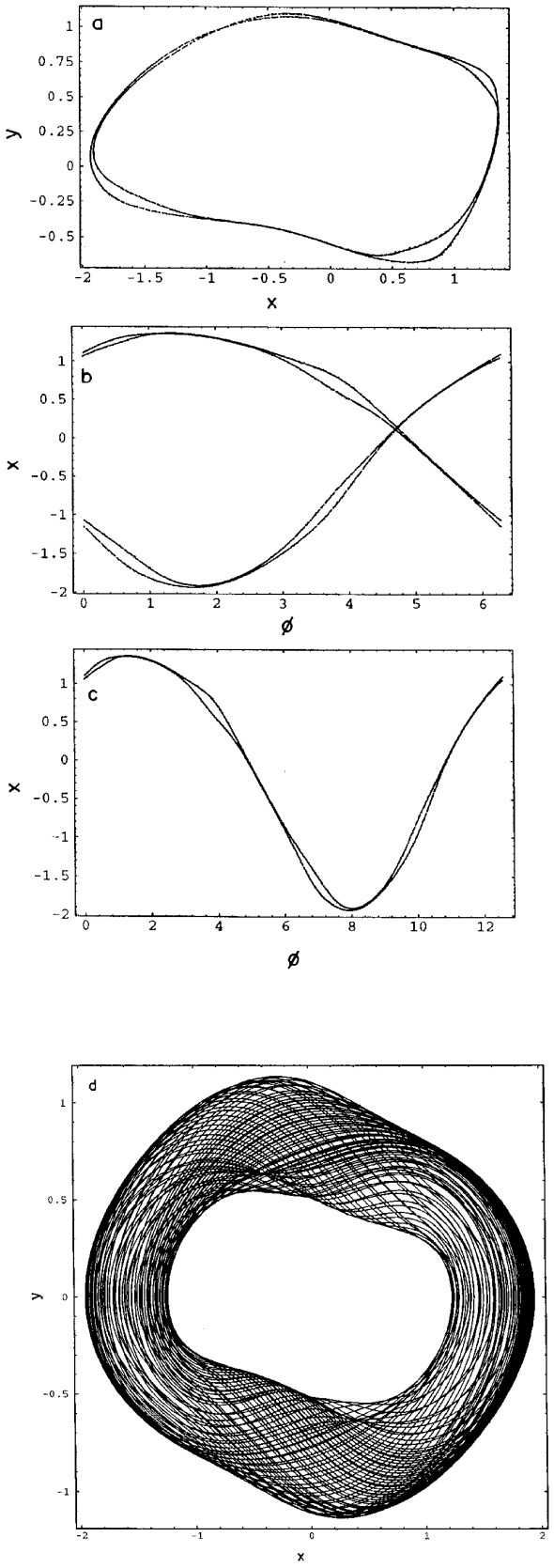

FIG. 6. Torus-doubled two-frequency quasiperiodic attractor for $\epsilon = 0.0317$. Details as in Fig. 5.

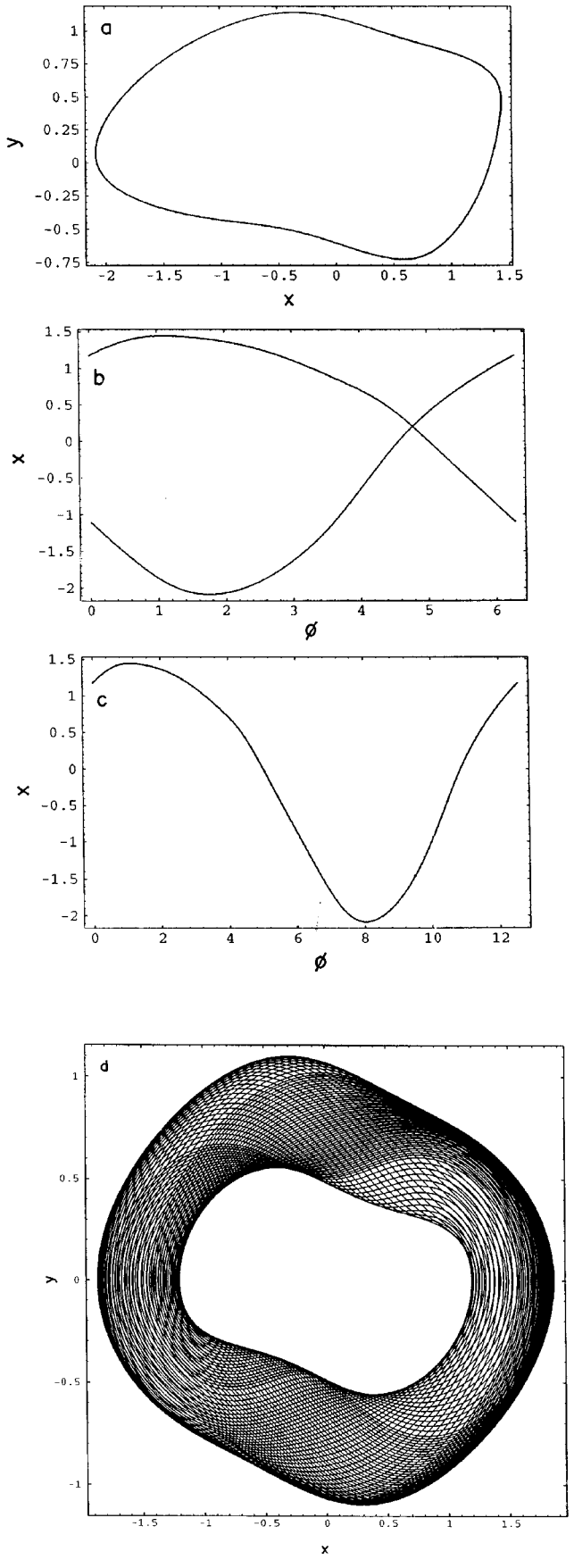

FIG. 7. Merged attractor for $\epsilon = 0.0353$. Details as in Fig. 5.

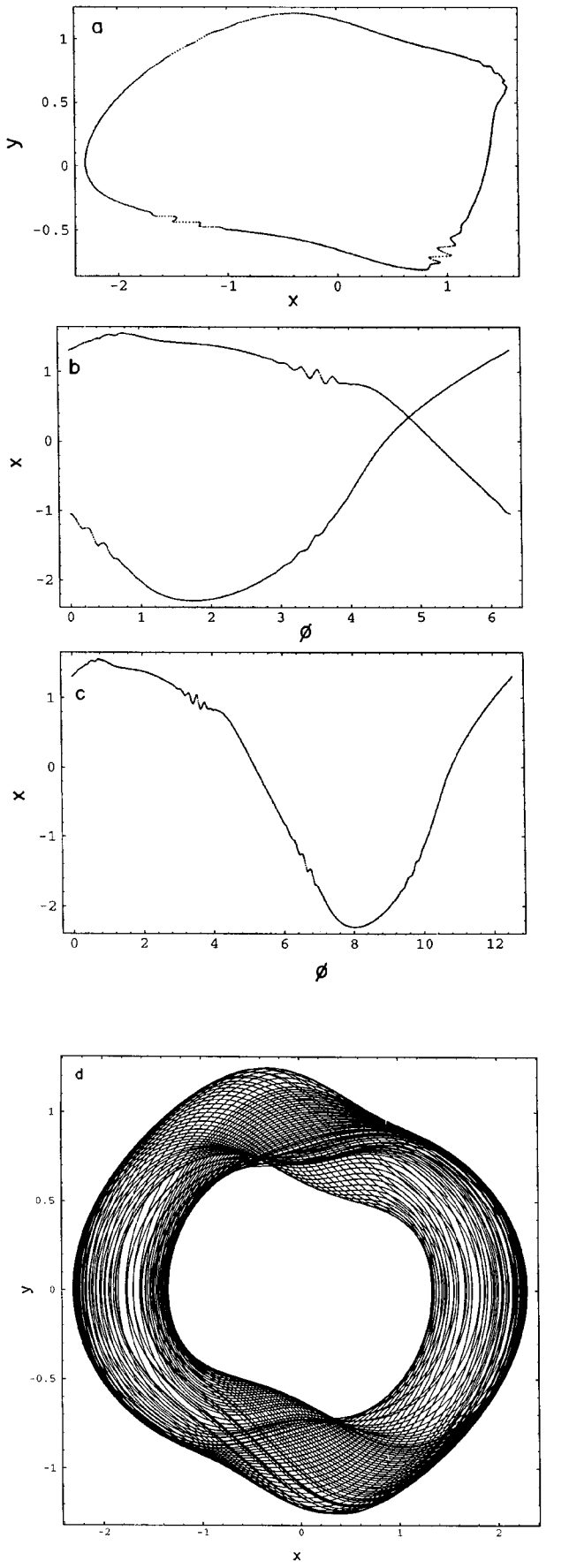

FIG. 8. Two-frequency attractor of Fig. 7 begins to wrinkle at $\epsilon = 0.0399$.

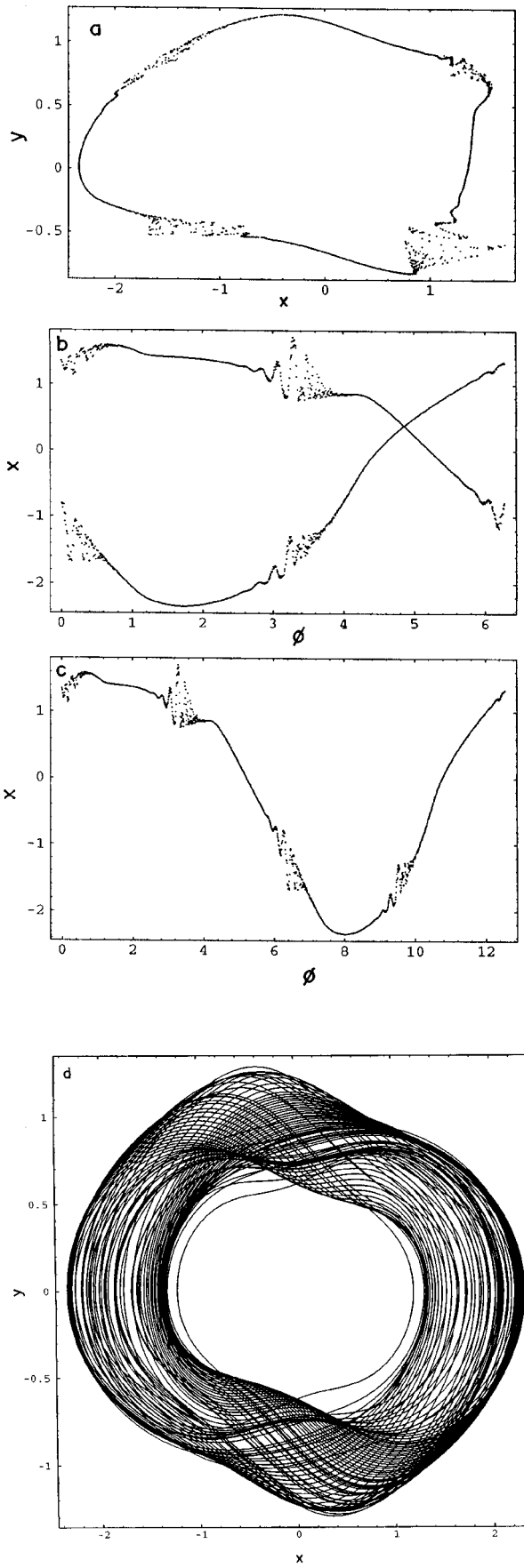

FIG. 9. Appearance of sharp bends at $\epsilon = 0.0408$.

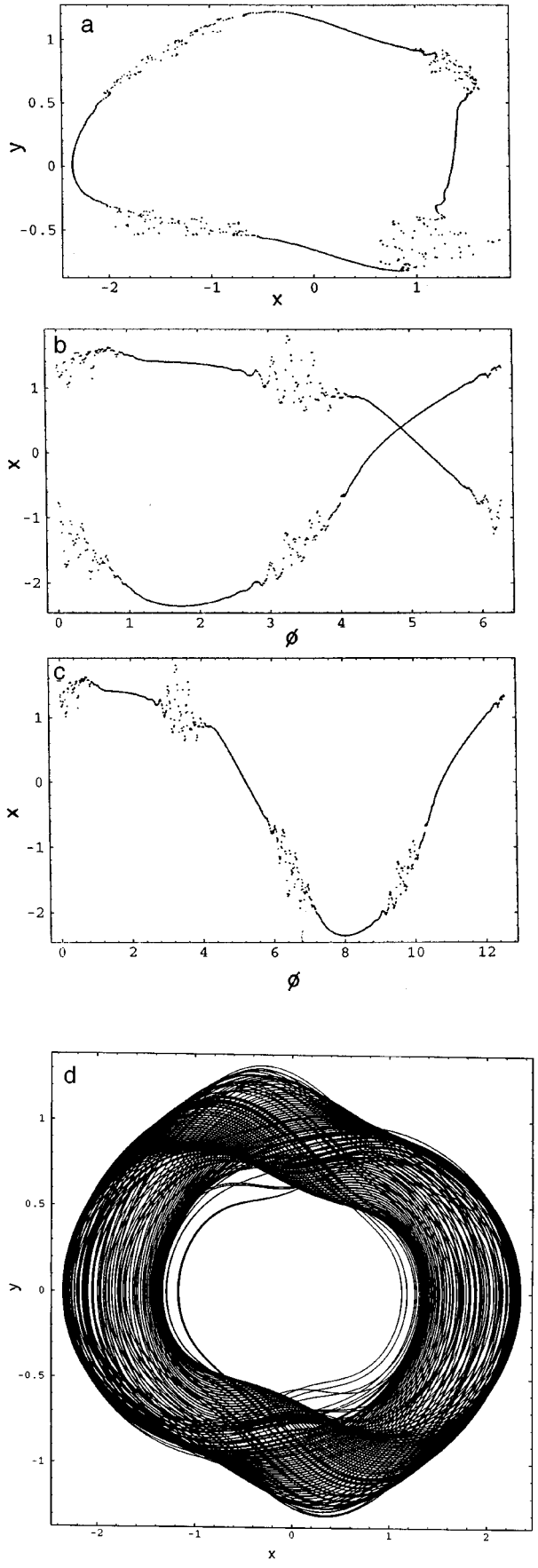

FIG. 10. Fully developed discontinuities on the two-frequency attractor for $\epsilon = 0.0410$.

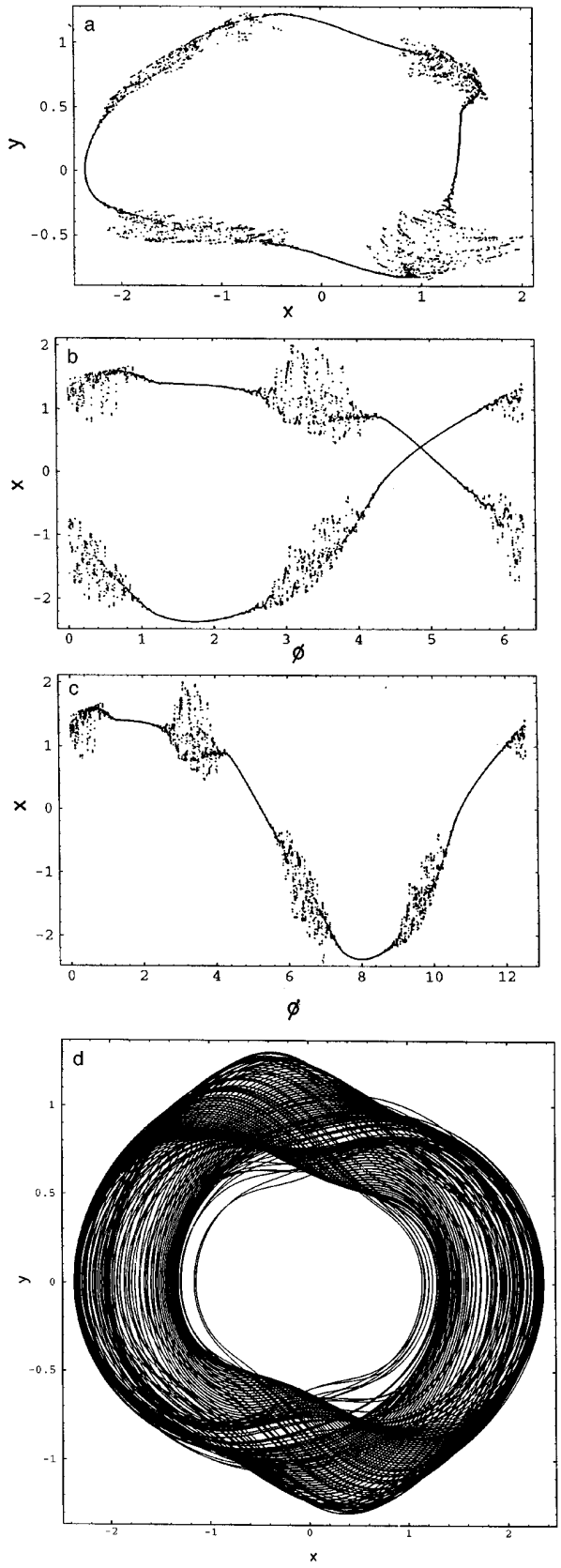

FIG. 11. Chaotic attractor at $\epsilon = 0.0413$.

where the values of the parameters are fixed as $\omega_0^2 = 0.25$, $\lambda = 0.5$, $\alpha = 0.2$, $\omega_p = 1.0$, $f = \omega_e = 0$, and $\Omega_0^2 = 6.7$, while ϵ is being varied. For small ϵ value, the attractor is a fixed point. For $\epsilon = 0.0146$, the attractor is a limit cycle of period 2 compared to the period of the parametric modulation $(= 2\pi/\omega_p)$. The period-2 nature may be understood from the considerations that the period of the parametric term $\cos\phi + \cos 2\phi$ is approximately twice the Poincaré period $T_p (= 2\pi/\omega_p)$. As ϵ is increased further to $\epsilon = 0.0487$, the attractor undergoes period doubling. On increasing the value of ϵ further, one observes a complete cascade of period-doubling bifurcations and a chaotic region as shown in Fig. 4.

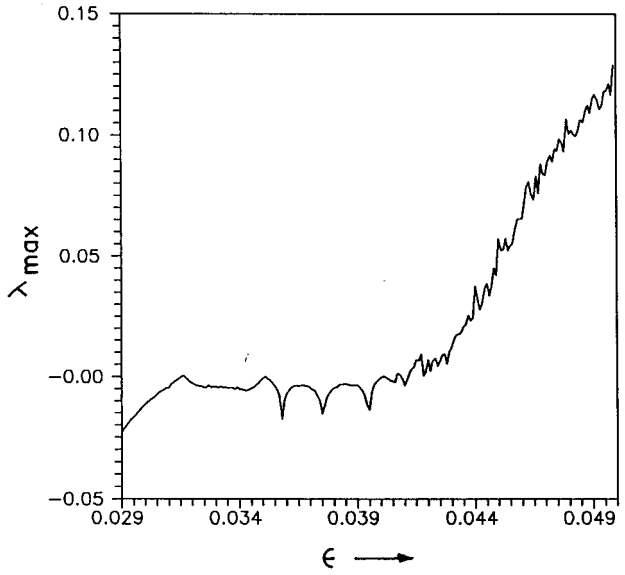

FIG. 12. Largest Lyapunov exponent vs ϵ, indicating torus doubling, merging, onset of discontinuities, and transition to chaos.

A. Torus doubling and merging bifurcations

Now we consider the combined effect of both the external and parametric forcing in Eq. (9). We choose the parameters f and ω_e to be 0.32 and 0.991, respectively, and vary the value ϵ. For $\epsilon = 0.03$, the attractor is a two-frequency quasiperiodic attractor (Fig. 5). As ϵ is increased to $\epsilon = 0.0317$, the attractor undergoes a torus-doubling bifurcation (as seen Fig. 6). We note from Figs. 5 and 6 that the two strands in the (x, ϕ) projection becomes four strands when torus doubling occurs. When we compute ϕ modulo 4π instead of modulo 2π during integration,we notice from Fig. 6 that the two bifurcated strands of length 2π in Fig. 6(b) are actually a single strand of length 4π [Fig. 6(c)]. As a result, it can be concluded that the torus doubling is nonetheless a length-doubling bifurcation. Further, it may be noted from Figs. 5(d) and 6(d) that each component of the bifurcated torus lies on the boundary of a Möbius band, a situation that is geometrically very similar to period-doubling bifurcations of periodic orbits in three-dimensional flows. A similar type of torus doubling has been observed in the quasiperiodically driven magnetoelastic ribbon experiment, double well Duffing oscillator and logistic map [17,22,23].

Interestingly, as ϵ is increased further to $\epsilon = 0.0353$, the strands of the length-doubled attractor begin to merge into a single attractor again as shown in Fig. 7.

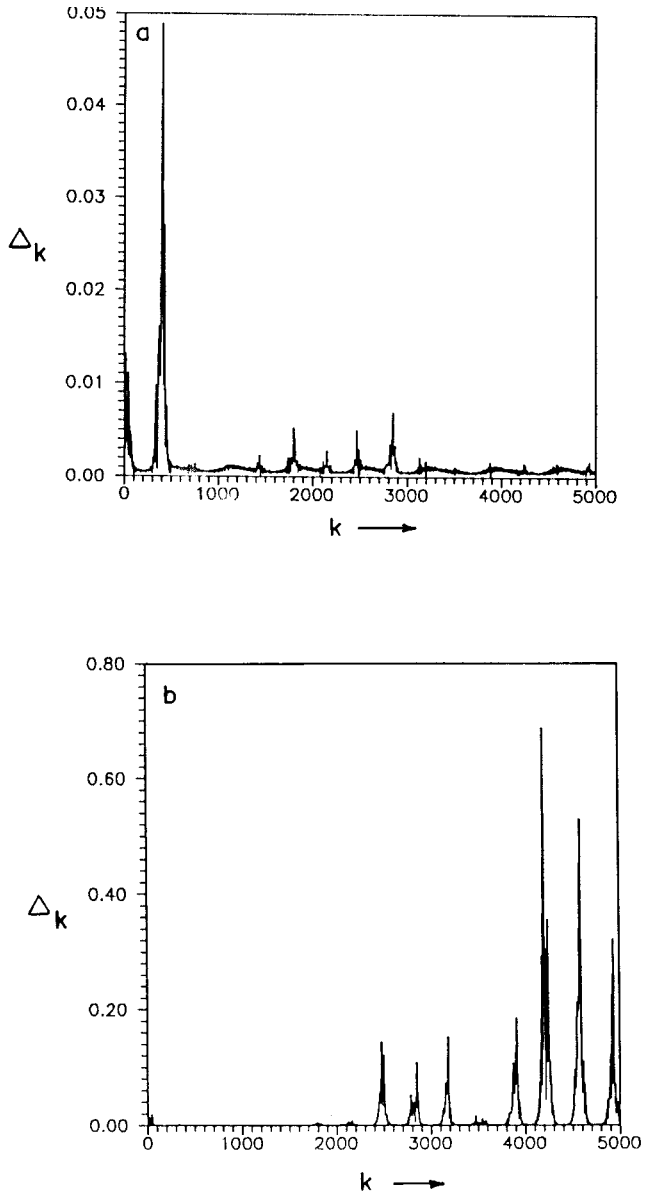

FIG. 13. Separation of two nearby points vs iteration. (a) Strange nonchaotic attractor ($\epsilon=0.0410$); (b) chaotic attractor ($\epsilon=0.0413$).

B. Strange nonchaotic and chaotic attractors

On increasing further the ϵ value to 0.0399 the merged attractor begins to wrinkle as shown in Fig. 8. Figure 9 reveals the formation of sharp bends in the strand of the attractor. These bends tend to become actual discontinuities at $\epsilon=0.041$. At such values, the attractor loses smoothness and becomes ''strange'' [17–28]. The attractor shown in Fig. 10 is nothing but nonchaotic as the maximum Lyapunov exponent works out to be $\lambda_1=-0.0123$. To confirm further about this behavior, we carry out some other characterizations below. On further increase of the value of ϵ to 0.0413, we find the emergence of a chaotic attractor, which though visibly similar to the nonchaotic strange attractor has a positive Lyapunov exponent ($\lambda_1=0.0013$). It is shown in Fig. 11. The chaotic behavior persists as the value of ϵ is increased further.

C. Characterization of nonchaotic and chaotic attractors

1. Lyapunov exponent

In Fig. 12, the largest Lyapunov exponent is plotted as a function of ϵ for a range of ϵ values. This figure summarizes the four major dynamical events that occur as the system is taken from two-frequency quasiperiodicity to chaos. The peak near $\epsilon=0.0317$ corresponds to the torus-doubling bifurcation. Such peaks in Lyapunov exponents are well-known occurrences at bifurcation points. The second peak near $\epsilon=0.0353$ corresponds to the torus merging bifurcation. The peak just beyond $\epsilon=0.0399$ coincides with the appearance of discontinuities on the attractor. The transition to chaos occurs at $\epsilon=0.0413$.

2. Correlation dimension

We have also estimated correlation dimension D_c of the attractors shown in Figs. 10 and 11, using the algorithm proposed by Grassberger and Proccacia [30]. The correlation dimension of the strange nonchaotic attractor shown in Fig. 10 is estimated as 1.77, while for the chaotic attractor of Fig. 11 it is 1.86.

3. Power spectral analysis

The occurrence of a strange nonchaotic attractor is further confirmed by a power spectrum analysis. For a strange nonchaotic attractor the number of peaks $N(\sigma)$ in a power spectrum exceeding a threshold amplitude σ scales [20] as

$$N(\sigma)\propto\sigma^{-\alpha},\quad 1<\alpha<2. \tag{10}$$

The power spectrum of the attractor is obtained using the fast Fourier transform with 8192 points. From the $\log_{10}N(\sigma)$ versus $\log_{10}(\sigma)$ plot the value of the scaling exponent is estimated as 1.63. This is in agreement with the power-law scaling relation (10).

4. Separation of nearby points

Sensitive dependence on initial conditions can be verified by looking at the separation Δ_k between two orbits starting from two nearby initial conditions. Two nearby points on the attractor (x_i,y_i,ϕ_i) and (x_j,y_j,ϕ_j) are chosen and their separation

$$\Delta_k=\sqrt{(x_{i+k}-x_{j+k})^2+(y_{i+k}-y_{j+k})^2} \tag{11}$$

is monitored at each forward step k. For regular behavior Δ_k will decay to zero as $t\to\infty$. However, it will vary irregularly with time for chaotic nature. Figure 13 is a plot of Δ_k versus k for two values, $\epsilon=0.0410$ and 0.0413. Figure 13(a) shows that Δ_k for the value $\epsilon=0.0410$ diminishes to zero after short-lived irregular variation. For comparison Fig. 13(b) shows that Δ_k for the value $\epsilon=0.0413$ exhibits more frequent and longer lived strong excursions. Hence the former case clearly supports the loss of sensitive dependence on initial conditions, which corresponds to the strange nonchaotic attractor, while the latter one corresponds to a chaotic attractor.

To sum up the above investigation, the attractor evolution has been found to follow the following route as ϵ is in-

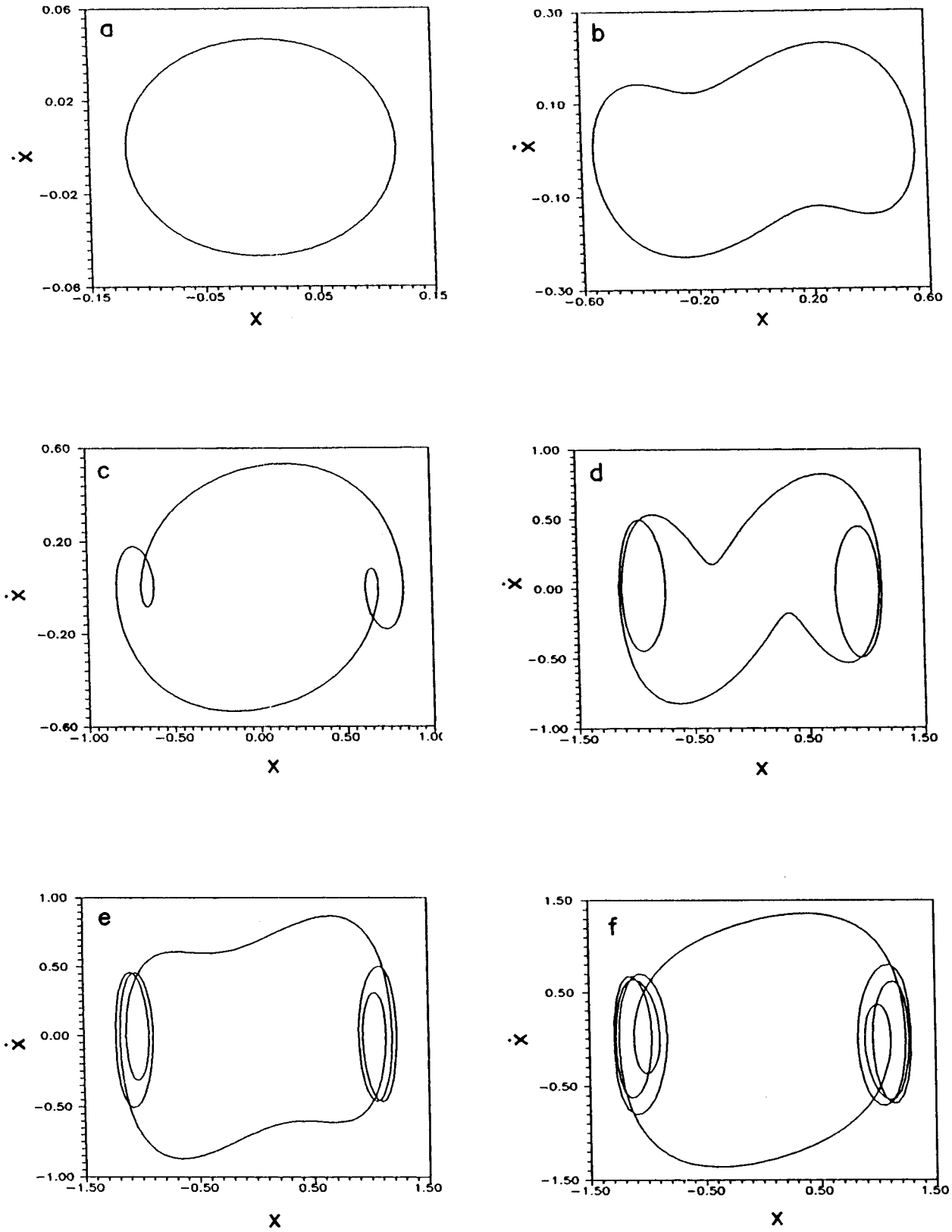

FIG. 14. Phase portrait (x-$\dot{x}$) of Eq. (6): (a) Symmetric period-T orbit at $f=0.213$; (b) asymmetric period-T orbit at $f=0.321$; (c) $f=0.537$; (d) $f=1.7$; (e) $f=2.832$; (f) $f=3.781$.

creased: two-frequency quasiperiodicity → torus doubling → torus merging → strange nonchaotic attractor → strange chaotic attractor.

This type of route to chaos seems to be rather different from the earlier studies on the torus-doubling route to chaos. In the earlier studies, it has been found that a variation of bifurcation parameter leads to the doubled torus, which gets wrinkled and becomes strange nonchaotic on touching the

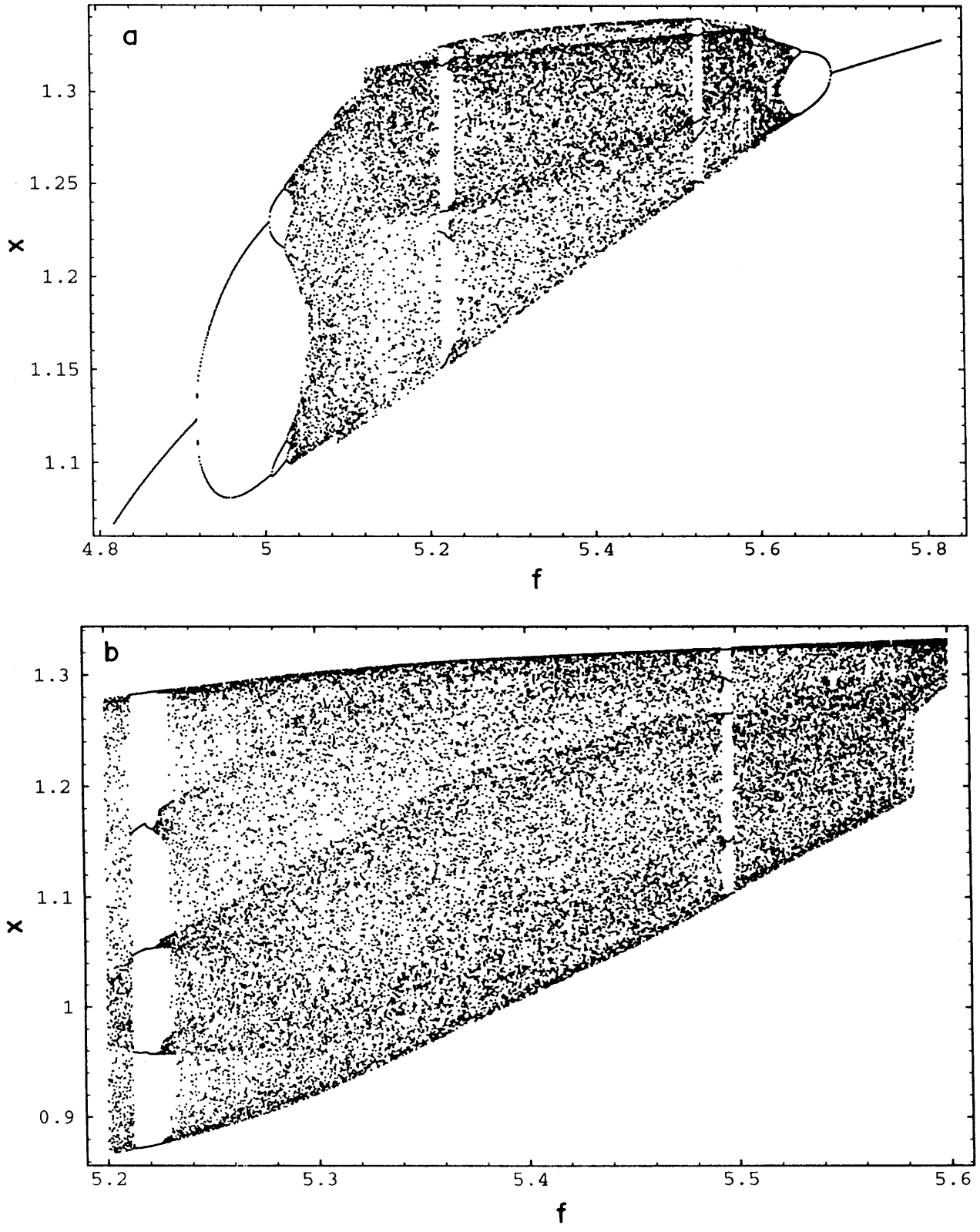

FIG. 15. Bifurcation diagram (f-x) of the system (6): (a) Period doubling, periodic windows, and period halving: $f \in (4.8,5.8)$; (b) period-5 bubble: $f \in (5.2,5.6)$. The other parameters are $\omega_0^2 = 1.0$, $\lambda = 0.5$, $\alpha = 0.2$, $\omega = 1.0$.

separatrix. However, in the present case, before the strange nonchaotic attractor appears, the doubled torus gets merged and then becomes wrinkled. Such a route to a strange nonchaotic attractor has very recently been investigated in a ring map [27,28]. Further, over a wide range of values of f and ϵ, it has been found that the system (8) also exhibits the other two known types of routes to chaos: (1) two-frequency quasiperiodicity $\rightarrow$ torus doubling $\rightarrow$ wrinkling $\rightarrow$ strange nonchaotic attractor $\rightarrow$ chaos; (2) two-frequency quasiperiodicity $\rightarrow$ strange nonchaotic attractor $\rightarrow$ chaos.

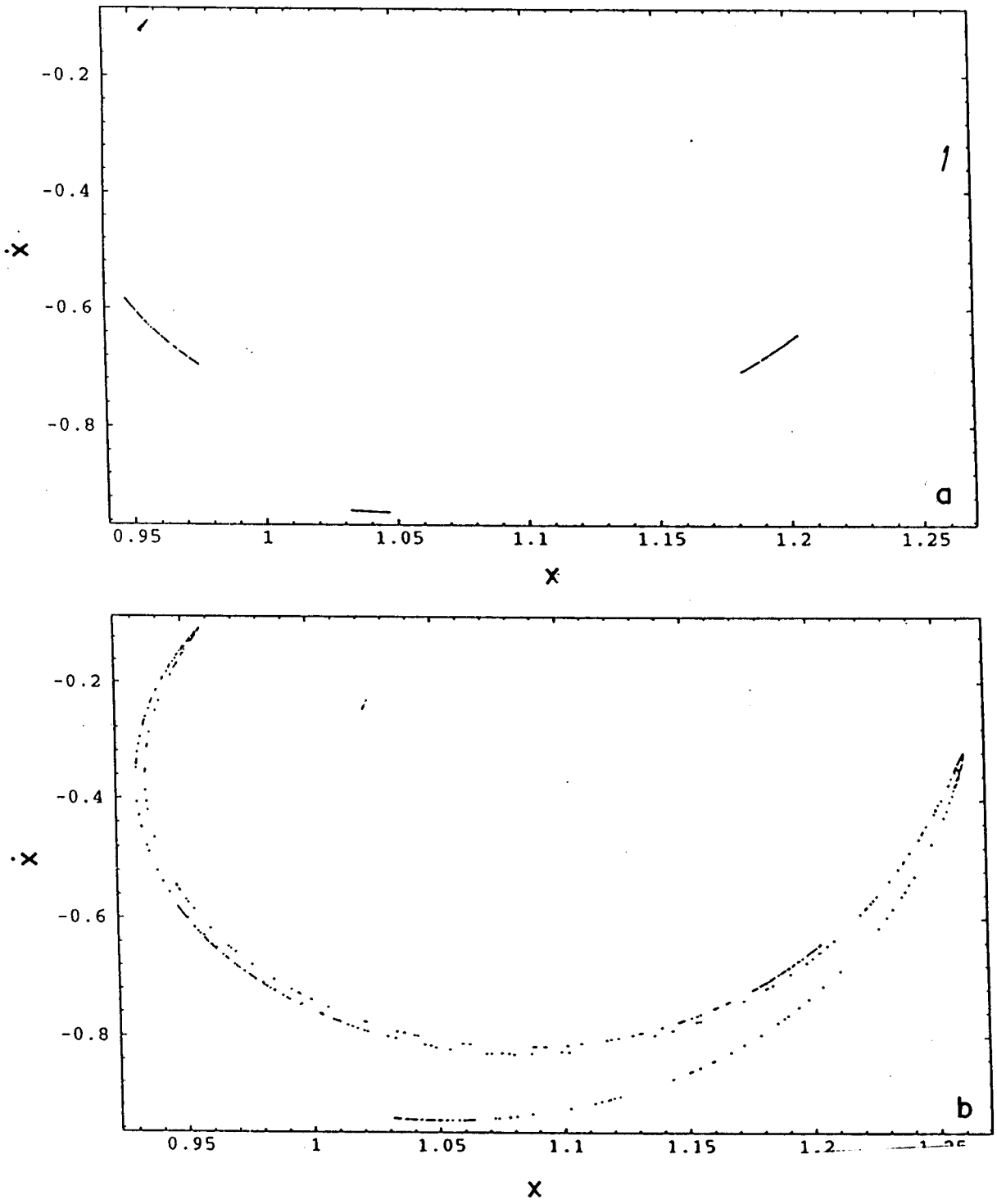

FIG. 16. Poincaré map in the $(x\text{-}\dot{x})$ plane of Eq. (6): (a) 5-band chaotic attractor at $f=5.2993$; (b) widened chaotic attractor at $f=5.2995$.

IV. CHAOTIC DYNAMICS OF THE NONLINEAR HARMONIC OSCILLATOR

Let us now consider the dynamics of the nonlinear harmonic oscillator under the influence of damped and driven forces. For this purpose, we integrate Eq. (6) numerically by keeping the parameters fixed as $\omega_0^2=1.0$, $\lambda=0.5$, $\alpha=0.2$, $\omega=1$, and vary the value of f.

For small values of f a stable fixed point occurs in the phase plane, which obviously corresponds to the damped oscillatory solution. At the value of $f=0.213$, a stable symmetrical limit cycle occurs. Further increasing the f value the symmetric orbit [Fig. 14(a)] loses its stability and a stable asymmetric orbit appears [Fig. 14(b)]. As the value of f is continuously increased further, changes in the number of loops in the $(x,\dot{x})$ plane (Fig. 14) occur.

When the driving value is increased to 4.8621, the first

period-doubling bifurcation is observed (Fig. 15). It is again preceded by a symmetry-breaking bifurcation.

On increasing the value of f further to 5.123, one observes a complete cascade of bifurcations and a chaotic region as shown in Fig. 15. The above chaotic region is interrupted by period-5 windows in the region $5.215 < f < 5.517$. Beyond the forcing value 5.623, as the value of f is increased, reverse bifurcations occur through period halvings (Fig. 15).

A. Antimonotonicity

Also we notice from Fig. 15(b) in the window region $5.215 < f < 5.517$, antimonotonicity can be observed in a way quite different from the one discussed in Sec. II. This can be clearly seen from the bifurcation diagram [Fig. 15(b)]. As f is increased a tangent bifurcation of the periodic orbit with period 5 is followed by a complete sequence of period-doubling bifurcations. Then after an interval with chaotic behavior, there is a reverse period-doubling sequence, ending in a periodic orbit with period 5. Such a pattern is called a period-5 bubble.

B. Crisis-induced intermittency

In the above range of the period-5 window, we also see that an attractor widening crisis occurs. When f is increased through $f_{*cs} = 5.2994$, the attractor undergoes a sudden change. The event causing this change is an interior crisis [29]. To see the reason behind it, we note that at the beginning of the window, there is a tangent bifurcation creating both period $5T$ attractor and unstable $5T$ orbit. At the crisis point $f = f_{*cs} = 5.2994$, the unstable period $5T$ collides with five pieces of the chaotic attractor (Fig. 16).

V. CONCLUSIONS

In this paper, we have shown that the velocity-dependent, damped, driven systems (5) and (6) exhibit a rich variety of bifurcations phenomena. It includes the familiar period-doubling bifurcations, preceded by a symmetry-breaking bifurcation. Besides the period-doubling route to chaos, intermittency, and antimonotonicity exist in the mechanical system (5) while in (6), antimonotonicity and crisis phenomena are observed. We have also investigated the dynamics of Eq. (8). Motivated by the detection of a strange nonchaotic attractor in experimental systems, we have also investigated the transition from smooth two-frequency quasiperiodicity behavior to strange nonchaotic (and chaotic) behavior as the driving parameter is increased. So far it is believed that the torus doubling followed by strange nonchaotic attractor is quite general. However, in the present case, a new type of transition, namely, the crisis of the torus (merging of doubled torus) results before the consequent appearance of a strange nonchaotic attractor.

ACKNOWLEDGMENTS

This work forms a part of research projects sponsored by the Department of Atomic Energy (NBHM) and the Department of Science and Technology, Government of India.

[1] N. V. Butenin, *Elements of the Theory of Nonlinear Oscillators* (Blaidsdell, New York, 1965).
[2] A. H. Nayfeh and D. T. Mook, *Nonlinear Oscillations* (Wiley, New York, 1979).
[3] P. M. Mathews and M. Lakshmanan, Quart. Appl. Math. **32**, 215 (1974).
[4] M. Lakshmanan, J. Phys. A **7**, 889 (1974).
[5] M. Lakshmanan, J. Sound Vib. **64**, 458 (1979).
[6] R. Delbourgo, Abdus Salam, and J. Strathdee, Phys. Rev. **187**, 1999 (1969).
[7] S. Gasiorowicz and D. Geffen, Rev. Mod. Phys. **41**, 531 (1969).
[8] U. Parlitz and W. Lauterborn, Phys. Lett. **107A**, 351 (1985).
[9] C. L. Olson and M. G. Olson, Am. J. Phys. **59**, 907 (1991).
[10] M. J. Feigenbaum, J. Stat. Phys. **19**, 25 (1978).
[11] Y. Pomeau and P. Mannevillie, Commun. Math. Phys. **74**, 189 (1980).
[12] I. Kan and J. A. Yorke, Bull. Am. Math. **23**, 469 (1990).
[13] P. S. Dawson, C. Grebogi, J. A. Yorke, I. Kan, and H. Kocak, Phys. Lett. A **162**, 1543 (1992).
[14] T. C. Newell, V. Kovanis, and A. Gannelides, Phys. Rev. Lett. **77**, 1747 (1996).
[15] M. Lakshmanan and K. Murali, *Chaos in Nonlinear Oscillators* (World Scientific, Singapore, 1996).
[16] E. Atlee Jackson, *Perspectives of Nonlinear Dynamics* (Cambridge University Press, New York, 1991).
[17] J. F. Heagy and W. L. Ditto, J. Nonlinear Sci. **1**, 423 (1991).
[18] K. Kaneko, Prog. Theor. Phys. **69**, 1806 (1983); **71**, 1112 (1984); **72**, 202 (1984).
[19] C. Grebogi, E. Ott, S. Pelikan, and J. A. Yorke, Physica D **13**, 261 (1984).
[20] F. J. Romeiras, A. Bondeson, E. Ott, T. M. Antonsen, and C. Grebogi, Physica D **26**, 277 (1987).
[21] F. J. Romeiras and E. Ott, Phys. Rev. A **35**, 4404 (1987).
[22] W. L. Ditto, M. L. Spano, H. T. Savage, S. N. Rauseo, J. F. Heagy, and E. Ott, Phys. Rev. Lett. **65**, 533 (1990).
[23] J. F. Heagy and S. M. Hammel, Physica D **70**, 140 (1994).
[24] T. Kapitaniak, Phys. Rev. E **47**, 1408 (1993).
[25] T. Kapitaniak and J. Wojewoda, *Attractors of Quasiperiodically Forced Systems* (World Scientific, Singapore, 1993).
[26] S. Rajasekar, Phys. Rev. E **51**, 775 (1995).
[27] V. S. Anishchenko, T. E. Vadivasova, and O. Sosnovtseva, Phys. Rev. E **53**, 4451 (1996).
[28] O. Sosnovtseva, U. Feudel, J. Kurths, and A. Pikovsky, Phys. Lett. A **218**, 255 (1996).
[29] C. Grebogi, E. Ott, F. J. Romeiras, and J. A. Yorke, Phys. Rev. A **36**, 5365 (1987).
[30] P. Grassberger and I. Proccacia, Physica D **13**, 34 (1984).